NEUROSCIENCE

Angiotensin-converting enzyme gates brain circuit–specific plasticity via an endogenous opioid

Brian H. Trieu[1,2], Bailey C. Remmers[3], Carlee Toddes[1], Dieter D. Brandner[1,2], Emilia M. Lefevre[3], Adrina Kocharian[1,2], Cassandra L. Retzlaff[3], Rachel M. Dick[1], Mohammed A. Mashal[3], Elysia A. Gauthier[3], Wei Xie[4], Ying Zhang[5], Swati S. More[4], Patrick E. Rothwell[3]*

Angiotensin-converting enzyme (ACE) regulates blood pressure by cleaving angiotensin I to produce angiotensin II. In the brain, ACE is especially abundant in striatal tissue, but the function of ACE in striatal circuits remains poorly understood. We found that ACE degrades an unconventional enkephalin heptapeptide, Met-enkephalin-Arg-Phe, in the nucleus accumbens of mice. ACE inhibition enhanced μ-opioid receptor activation by Met-enkephalin-Arg-Phe, causing a cell type–specific long-term depression of glutamate release onto medium spiny projection neurons expressing the Drd1 dopamine receptor. Systemic ACE inhibition was not intrinsically rewarding, but it led to a decrease in conditioned place preference caused by fentanyl administration and an enhancement of reciprocal social interaction. Our results raise the enticing prospect that central ACE inhibition can boost endogenous opioid signaling for clinical benefit while mitigating the risk of addiction.

As neural circuit dysfunction in brain disorders becomes increasingly well defined, there is a growing need for interventions that specifically target dysfunctional circuit elements (*1*). Multiple brain disorders (*2*–*4*) involve imbalanced output of nucleus accumbens (NAc) medium spiny projection neurons expressing dopamine receptor Drd1 (D1-MSNs) or Drd2 (D2-MSNs). This imbalance has proven difficult to correct with standard interventions because these two MSN subtypes are physically intermingled, receive synaptic inputs from common sources, and have similar molecular profiles. A rare exception is ACE (angiotensin-converting enzyme), which exhibits enriched expression by D1-MSNs in the dorsal striatum (*5*, *6*) and the NAc (table S1 and fig. S1). Inhibitors of ACE and other peptidases can be combined to regulate striatal excitatory synaptic transmission in an opioid-dependent fashion (*7*); this finding suggests that in addition to angiotensin conversion, ACE cleaves and degrades a peptide ligand for opioid receptors (Fig. 1A).

To separately measure how ACE inhibition affects excitatory synaptic transmission onto D1-MSNs and D2-MSNs, we performed whole-cell recordings in acute NAc brain slices from double-transgenic Drd1-tdTomato/Drd2-eGFP reporter mice (Fig. 1C and fig. S2). Brief exposure to 10 μM captopril, a prototypical ACE inhibitor (*8*), caused long-term depression (captopril-LTD) of excitatory synaptic transmission onto D1-MSNs (Fig. 1D). Captopril did not alter excitatory synaptic transmission onto D2-MSNs, which express ACE at a lower level than D1-MSNs (table S1 and fig. S1). There was also no effect of captopril at excitatory synapses onto layer V pyramidal neurons in the anterior cingulate cortex (fig. S3), where ACE expression is low (*5*, *6*).

Captopril and other ACE inhibitors canonically block conversion of angiotensin I to angiotensin II, preventing activation of the angiotensin II type 1 receptor (AT1R) and increasing levels of angiotensin I (Fig. 1B). However, LTD was not observed in D1-MSNs exposed to valsartan (2 to 20 μM), an AT1R antagonist, or exogenous angiotensin I peptide (1 μM) (Fig. 1E). In contrast, captopril-LTD in D1-MSNs was blocked in the continuous presence of 10 μM naloxone, an opioid receptor antagonist, but was not reversed by chasing captopril with naloxone (Fig. 1F). Captopril-LTD in D1-MSNs was associated with an increase in paired-pulse ratio and a decrease in $1/CV^2$ (Fig. 1, G to I), two changes that indicate a decreased presynaptic probability of glutamate release, likely due to activation of presynaptic opioid receptors (*7*).

Local release of enkephalin peptides by D2-MSNs can regulate excitatory synaptic input to D1-MSNs (*9*). ACE can cleave enkephalin peptides but is not principally responsible for degrading conventional Met-enkephalin or Leu-enkephalin in brain tissue (*10*). The pro-enkephalin gene (*Penk*) also encodes Met-enkephalin-Arg-Phe (MERF), a heptapeptide abundant in the NAc (*11*). MERF has high binding affinity for opioid receptors (*12*), is more potent than Met-enkephalin (*13*), and can be degraded by ACE (*14*). Using liquid chromatography–tandem mass spectrometry (LC-MS/MS), we simultaneously quantified extracellular levels of enkephalins and other neuropeptides (*15*) released from mouse brain slices (Fig. 2A and fig. S4). After stimulation with KCl (50 mM), we observed increased extracellular levels of MERF as well as Met-enkephalin and Leu-enkephalin, along with dynorphins and substance P (Fig. 2B). Concentrations of MERF released from isolated NAc tissue punches were higher than those from dorsal striatum tissue punches (fig. S5, A to D). We could not detect an appreciable release of angiotensin II (Fig. 2B) or bradykinin (fig. S5E). Enkephalin signals were absent in constitutive *Penk* knockout mice (fig. S5, F to K), which indicates that *Penk* is the primary source of enkephalin in this preparation.

Inhibition of ACE with 10 μM captopril robustly increased extracellular levels of MERF without affecting conventional enkephalins or other neuropeptides (Fig. 2C and table S2). We observed similar effects using trandolaprilat, a different ACE inhibitor that also caused LTD of excitatory synaptic input to D1-MSNs (fig. S6). In contrast, extracellular levels of MERF were not affected by pharmacological inhibition of aminopeptidase N and neprilysin, the enzymes responsible for degrading conventional enkephalins (*10*) (fig. S7A). A cocktail of inhibitors for all three enzymes blocked degradation of enkephalins as well as other neuropeptides (fig. S7B). D2-MSNs express high levels of *Penk* (*6*), making them a likely source of MERF. To evaluate this possibility, we bred mice with genetic expression of channelrhodopsin-2 in D2-MSNs (Fig. 2D and fig. S8). Optogenetic stimulation of acute brain slices from these mice increased extracellular levels of conventional enkephalins, but only MERF levels were elevated in the presence of captopril (Fig. 2, E and F, and table S3).

To investigate how MERF regulates NAc synaptic transmission, we measured miniature excitatory postsynaptic currents (mEPSCs; fig. S9). Increasing concentrations of MERF caused a dose-dependent decrease in mEPSC frequency without altering mEPSC amplitude (Fig. 3, A and B), consistent with a presynaptic reduction of glutamate release probability. Both MERF and Met-enkephalin (fig. S10, A to C) had similar effects on D1-MSNs and D2-MSNs, which suggests that presynaptic terminals onto both cell types are equally sensitive to endogenous opioids. We used these data to construct dose-response curves and found that MERF [half-maximal inhibitory concentration (IC_{50}) = 438 nM; Fig. 3C] was more potent than Met-enkephalin (IC_{50} = 993 nM; fig. S10D), as previously reported (*13*).

These experiments identified a threshold MERF concentration (100 nM) that did not reliably affect synaptic transmission. Captopril alone (10 μM) also had no effect on frequency or amplitude of mEPSCs, which are measured

[1]Graduate Program in Neuroscience, University of Minnesota Medical School, Minneapolis, MN, USA. [2]Medical Scientist Training Program, University of Minnesota Medical School, Minneapolis, MN, USA. [3]Department of Neuroscience, University of Minnesota Medical School, Minneapolis, MN, USA. [4]Center for Drug Design, College of Pharmacy, University of Minnesota, Minneapolis, MN, USA. [5]Minnesota Supercomputing Institute, University of Minnesota, Minneapolis, MN, USA.
*Corresponding author. Email: rothwell@umn.edu

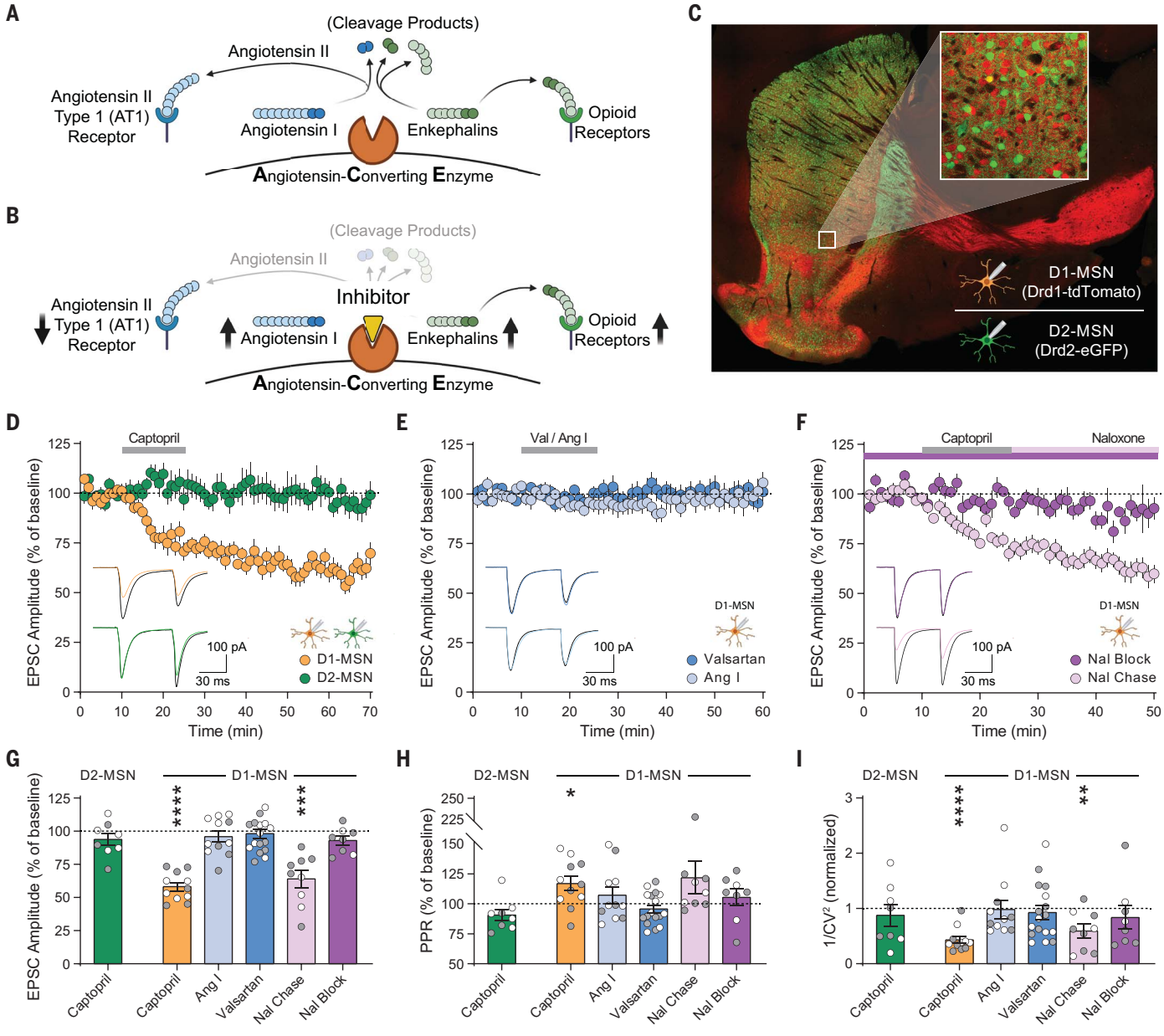

Fig. 1. ACE inhibition reduces excitatory input to D1-MSNs via endogenous opioid signaling. (**A** and **B**) Schematic of angiotensin and enkephalin regulation by ACE, in the absence (A) and presence (B) of ACE inhibition. (**C**) Drd1-tdTomato expression (red) in D1-MSNs, and Drd2-eGFP expression (green) in D2-MSNs; box size is 250 μm × 250 μm. (**D** to **F**) EPSC amplitude before, during, and after 15-min bath perfusion (gray bar) of 10 μM captopril in D1-MSNs (orange, $n = 11$) or D2-MSNs (green, $n = 8$) (D); AT1R antagonist valsartan [dark blue, 2 μM ($n = 8$) and 20 μM ($n = 9$)] or 1 μM angiotensin I peptide (light blue, $n = 11$) in D1-MSNs (E); or 10 μM captopril in continual presence of opioid receptor antagonist naloxone (10 μM, dark purple, $n = 8$) or chased by naloxone (10 μM, light purple, $n = 9$) in D1-MSNs (F). Insets show traces before (black lines) and after (last 5 min of recording, colored lines). (**G** to **I**) EPSC parameters during the last 5 min of each recording, expressed as percentage of baseline prior to drug application: EPSC amplitude (G), paired-pulse ratio (H), and $1/CV^2$ (I). Data are means ± SEM for all panels; open and solid circles in (G) to (I) indicate recordings from female and male mice, respectively. *$P < 0.05$, **$P < 0.01$, ***$P < 0.001$, ****$P < 0.0001$ [analysis of variance (ANOVA) followed by one-sample t test versus baseline]; see data S1 for complete statistics.

in the absence of stimulation required to release endogenous opioids (*7*, *9*). However, the combination of captopril and a threshold MERF concentration caused synergistic depression of mEPSC frequency in D1-MSNs, but not D2-MSNs (Fig. 3, D and E, and fig. S11). This effect was absent after conditional genetic deletion of ACE from D1-MSNs (fig. S12). Inhibitors of aminopeptidase N and neprilysin did not enhance the effects of MERF but did potentiate the effects of a threshold concentration of Met-enkephalin (100 nM) in both D1-MSNs and D2-MSNs (fig. S10, E to I).

To determine the opioid receptor subtype engaged by ACE inhibition, we recorded mEPSCs in D1-MSNs and applied captopril (10 μM) with threshold MERF (100 nM) in the presence of selective opioid receptor antagonists. Blocking δ-opioid receptors with SDM25N (500 nM) or κ-opioid receptors with NOR-BNI (100 nM) did not prevent the decrease in mEPSC frequency (Fig. 3F and fig. S13). However, this effect was completely blocked by the μ-opioid receptor (MOR) antagonist CTAP (1 μM), with no change

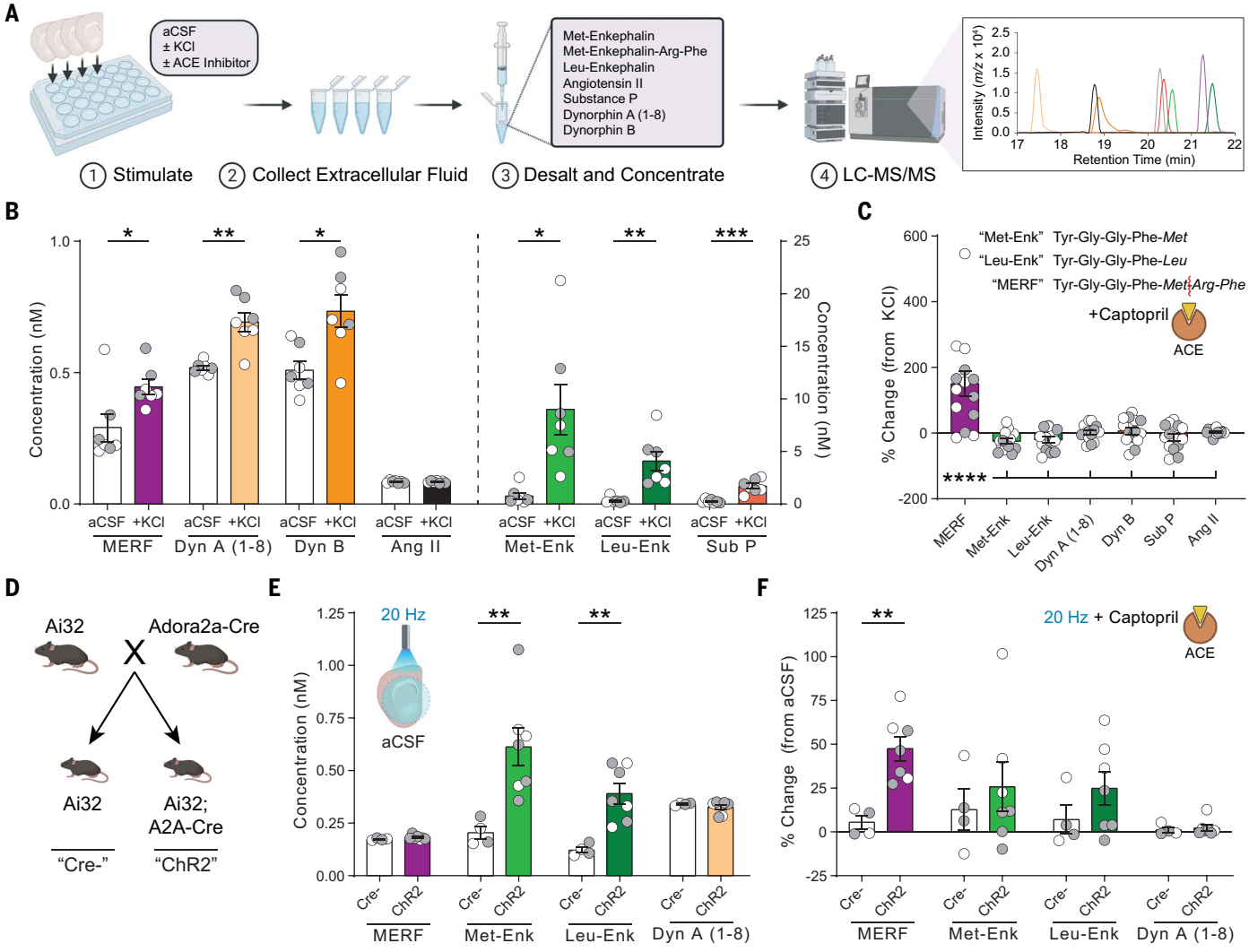

Fig. 2. ACE selectively degrades MERF in the extracellular space. (**A**) Quantification of neuropeptide release from brain slices using LC-MS/MS. (**B**) Extracellular neuropeptide levels from slices submerged in normal aCSF or 50 mM KCl. (**C**) Percent change in extracellular neuropeptide levels after KCl stimulation in presence versus absence of 10 μM captopril. Inset: Enkephalin amino acid sequences and site of enzymatic cleavage of MERF by ACE (red line). (**D**) Breeding strategy to generate mice expressing channelrhodopsin-2 in D2-MSNs. (**E**) Extracellular neuropeptide levels from slices after optogenetic stimulation at 20 Hz. (**F**) Percent change in extracellular neuropeptide levels after optogenetic stimulation in presence versus absence of 10 μM captopril. Data are means ± SEM for all panels; open and solid circles indicate samples from female and male mice, respectively. *$P < 0.05$, **$P < 0.01$, ***$P < 0.001$, ****$P < 0.0001$ [ANOVA followed by simple effect test in (B), (E), and (F) or Fisher's LSD post hoc test in (C)]; see data S1 for complete statistics.

in mEPSC amplitude (Fig. 3F and fig. S14, A to D). To confirm the role of MOR, we crossed Drd1-tdTomato reporter mice with constitutive MOR (*Oprm1*) knockout mice, generating offspring that lacked functional MOR ($Oprm1^{-/-}$) as well as littermate controls ($Oprm1^{+/+}$) (fig. S14E). The synergistic effect of captopril (10 μM) and threshold MERF (100 nM) on mEPSC frequency in D1-MSNs was absent from $Oprm1^{-/-}$ mice (Fig. 3, G and H, and fig. S14, F to I). Captopril-LTD of evoked EPSCs in D1-MSNs was also absent from $Oprm1^{-/-}$ mice (Fig. 3, I and J). MOR is also expressed postsynaptically by most D1-MSNs and fewer D2-MSNs (*16*, *17*). In current-clamp recordings, 1 μM MERF decreased action potential firing in D1-MSNs (Fig. 3K) but not D2-MSNs (fig. S15A). In combination with 10 μM captopril, a threshold MERF concentration (100 nM) also decreased action potential firing in D1-MSNs (Fig. 3L) but not D2-MSNs (fig. S15B).

Our experiments in brain slices have shown that ACE inhibition reduces excitatory synaptic input to D1-MSNs (Fig. 4A). To complement these analyses, we used fiber photometry in vivo and found that systemic captopril administration reduced the sensitivity of D1-MSNs to optogenetic stimulation of excitatory input arising from the medial prefrontal cortex (mPFC; Fig. 4, B to D, and fig. S16). Because the rewarding effects of addictive drugs are driven by D1-MSN activity and strengthening of excitatory synaptic input (*18*–*22*), we used an unbiased place-conditioning assay to determine whether systemic captopril administration could counteract the rewarding properties of fentanyl (Fig. 4E). Mice exhibited robust conditioned place preference (CPP) for a fentanyl-paired context [0.04 mg/kg subcutaneously (s.c.)], but the magnitude of CPP was significantly attenuated when captopril [30 mg/kg intraperitoneally (i.p.)] was injected before fentanyl (Fig. 4, F and G). Trandolapril (the prodrug form of trandolaprilat) had a similar effect on fentanyl CPP (fig. S17). Captopril itself was not rewarding or aversive in the place-conditioning assay (Fig. 4, H to J) and did not alter locomotion during conditioning (fig. S18). In a test of social interaction between two freely moving mice, captopril administration increased the amount of social interaction (Fig. 4, K to O),

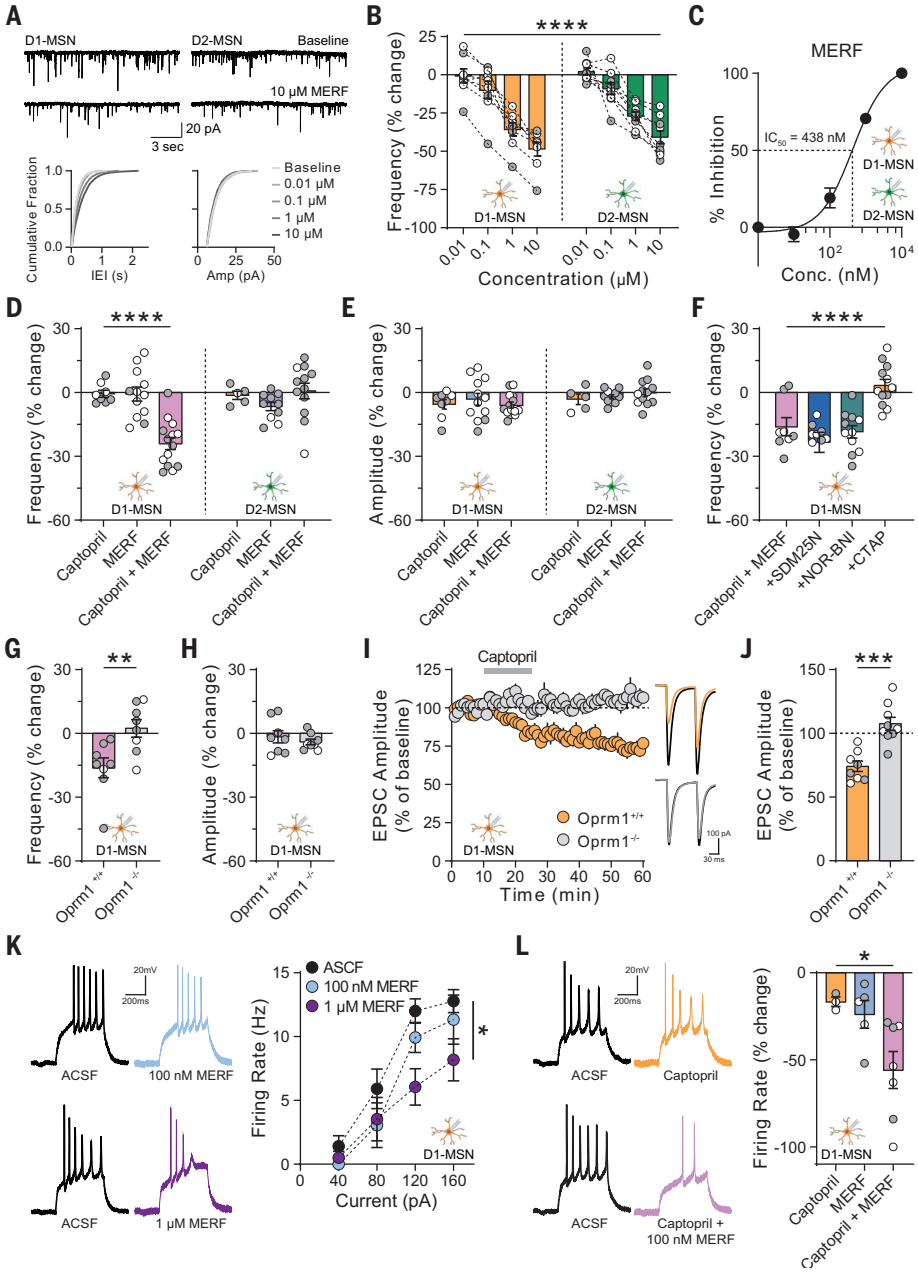

Fig. 3. Captopril enhances MERF effects on presynaptic and postsynaptic opioid receptors. (**A**) Top: mEPSCs from D1-MSNs (left) and D2-MSNs (right) before and after bath perfusion of 10 μM MERF. Bottom: Cumulative fraction plots of interevent interval (left) and amplitude (right) of mEPSCs at increasing MERF concentrations (0.01 to 10 μM). (**B**) MERF causes a dose-dependent decrease in mEPSC frequency in D1-MSNs (left, orange, $n = 8$) and D2-MSNs (right, green, $n = 9$). (**C**) Sigmoidal interpolation of MERF dose response normalized to maximal frequency change at 10 μM (IC_{50}, 438 nM; 95% confidence interval, 279 to 690 nM; $n = 17$). (**D** and **E**) mEPSC frequency (D) and amplitude (E) after combined captopril (10 μM) and/or threshold MERF (100 nM) in D1-MSNs (left, $n = 14$) and D2-MSNs (right, $n = 12$). (**F**) Combined effect of captopril and threshold MERF in the presence of selective antagonists of δ (SDM25N, 500 nM, blue, $n = 9$), κ (NOR-BNI, 100 nM, green, $n = 11$), or μ (CTAP, 1 μM, orange, $n = 12$) opioid receptors. (**G** and **H**) Combined effect of captopril and threshold MERF on mEPSC frequency (G) and amplitude (H) in $Oprm1^{-/-}$ knockout mice (gray, $n = 8$) and $Oprm1^{+/+}$ littermates (purple, $n = 8$). (**I** and **J**) EPSC amplitude time course (I) or average during last 5 min (J) of captopril-LTD in $Oprm1^{+/+}$ (orange, $n = 8$) and $Oprm1^{-/-}$ mice (gray, $n = 9$). Inset shows traces before captopril (black lines) and during last 5 min (colored lines). (**K**) Action potential firing rate of D1-MSNs ($n = 5$ to 7) before and after exposure to MERF (0.1 to 1 μM). (**L**) Change in action potential firing rate of D1-MSNs ($n = 3$ to 7) at 120 pA after combined captopril (10 μM) and/or threshold MERF (100 nM). Data are means ± SEM for all panels; open and solid circles indicate recordings from female and male mice, respectively. $^*P < 0.05$, $^{**}P < 0.01$, $^{***}P < 0.001$, $^{****}P < 0.0001$ [concentration main effect in (B), treatment simple effect in D1-MSNs in (D), genotype or treatment main effect in (F), (J), (K), and (L), two-sample t test in (G)]; see data S1 for complete statistics.

which is consistent with enhanced MOR signaling in the NAc (*22*) and rules out a general disruption of motivated behavior.

Targeting molecules with enriched expression in specific circuit elements is one strategy for translating an increasingly precise understanding of neural circuit function into therapeutic advances (*1*). Our data show that enriched expression of ACE by D1-MSNs can be leveraged to induce synaptic plasticity in a brain circuit–specific fashion (fig. S19). Pharmacological inhibition of ACE prevents degradation of MERF, thereby enhancing endogenous MOR signaling in the NAc (Fig. 4A). This resembles the effects of selective reuptake inhibitors for other neurotransmitters, which have substantial therapeutic value for brain disorders. The circuit specificity of these effects likely results from the high levels of MERF in the NAc, combined with enriched expression of ACE by D1-MSNs. ACE inhibition did not induce synaptic plasticity at excitatory synapses onto D2-MSNs or layer V pyramidal cells in the ACC, even though these synapses were sensitive to exogenous MERF application (Fig. 3B and fig. S3). By selectively and locally enhancing endogenous opioid signaling in the vicinity of D1-MSNs, central ACE inhibition may limit abuse liability by avoiding MOR activation in other brain circuits. Indeed, systemic ACE inhibition significantly reduced the rewarding effects of fentanyl and increased reciprocal social interaction. Conversely, rodents that exhibit reduced social interaction after chronic social stress have up-regulated ACE expression in NAc tissue (*23*) and D1-MSNs (*24*). This behavioral phenotype is reversed by treatment with antidepressant drugs (*25*), and human patients taking centrally active ACE inhibitors can experience relief from depression (*26*–*28*) as well as improved quality of life (*29*, *30*) and slower cognitive decline (*31*). Together, this evidence suggests that central ACE inhibition could have therapeutic potential for a variety of brain conditions. Our findings may thus herald a new era of repositioning and redesigning ACE inhibitors with central activity as a brain circuit–specific pharmacotherapy.

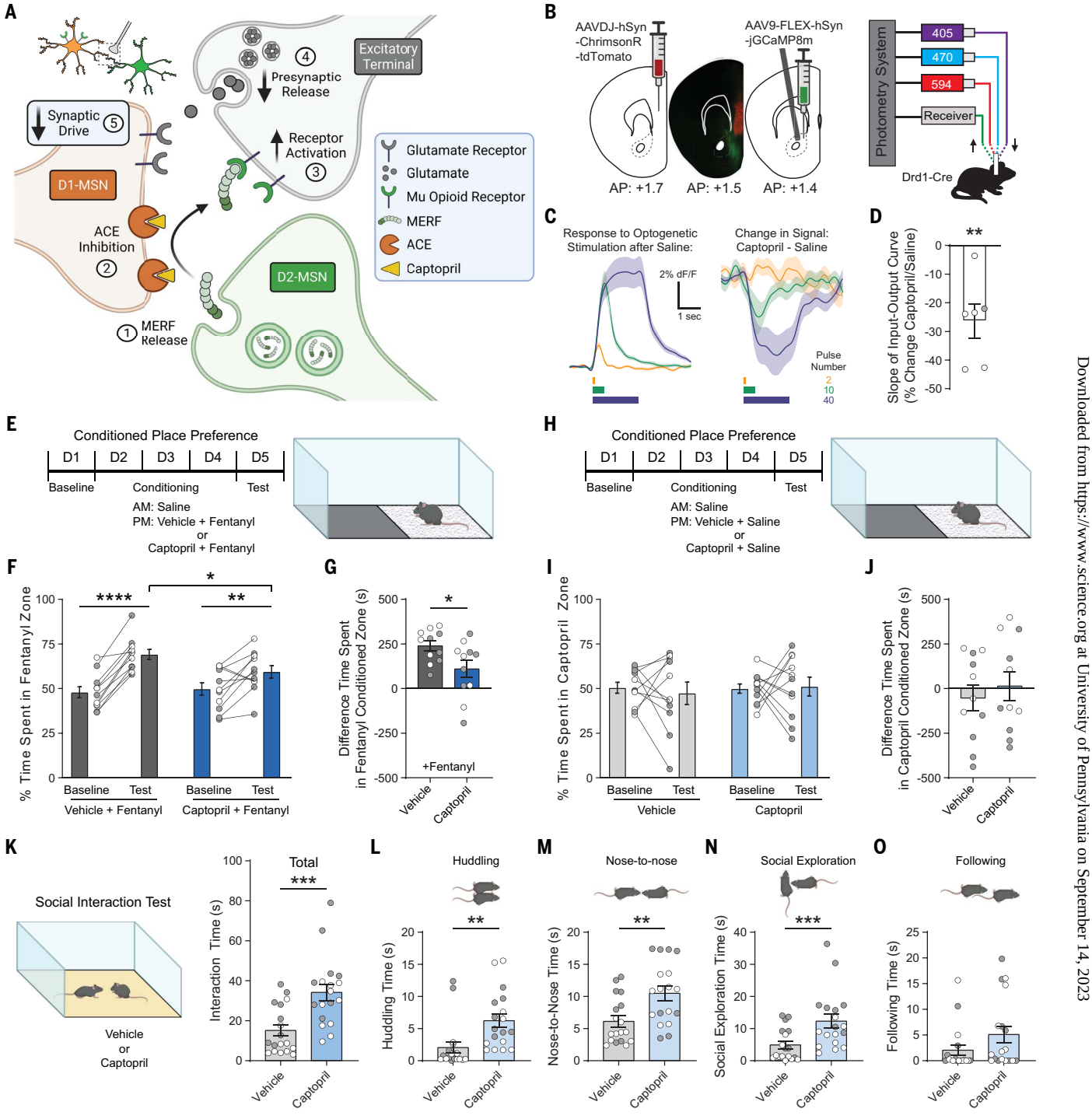

Fig. 4. Systemic captopril reduces excitatory input to D1-MSNs, counteracts fentanyl reward, and increases sociability. (**A**) Proposed mechanism by which captopril regulates glutamate release onto D1-MSNs via MERF. (**B**) Left: Schematic showing viral injection of ChrimsonR-tdTomato in mPFC and Cre-dependent GCaMP8m in NAc, separated by fluorescent image showing viral expression. Right: Setup for simultaneous optogenetic stimulation (594 nm) and fiber photometry recording (405/470 nm). (**C**) Left: Traces showing average response to 2, 10, and 40 pulses of red light at 20 Hz after injection of saline. Right: Average change in response after injection of captopril (30 mg/kg i.p.). (**D**) Percent change in slope of the input-output curve after injection of captopril versus saline (n = 6). (**E** to **G**) Schematic of unbiased place conditioning procedure (E), with percent time on fentanyl side (F) and CPP score (G) for groups receiving fentanyl (0.04 mg/kg s.c.) preceded by vehicle (n = 11, dark gray) or captopril (30 mg/kg i.p.; n = 11, dark blue). (**H** to **J**) Schematic of unbiased place conditioning procedure (H), with percent time on fentanyl side (I) and CPP score (J) for groups receiving saline preceded by vehicle (n = 11, gray) or captopril (30 mg/kg i.p.; n = 11, blue). (**K**) Left: Schematic of reciprocal social interaction test after injection of vehicle or captopril (30 mg/kg i.p.). Right: Total social interaction time after vehicle (n = 18, gray) or captopril (n = 18, blue). (**L** to **O**) Time spent huddling (L), interacting nose-to-nose (M), socially exploring (N), or following (O) the partner mouse throughout the assay. Data are means ± SEM for all panels; open and solid circles indicate female and male mice, respectively. *P < 0.05, **P < 0.01, ***P < 0.001, ****P < 0.0001 [one-sample t test in (D), simple effect of session/treatment in (F), treatment main effect in (G) and (K) to (N)]; see data S1 for complete statistics.

REFERENCES AND NOTES

1. J. A. Gordon, *Nat. Neurosci.* **19**, 1385–1386 (2016).
2. P. E. Rothwell *et al.*, *Cell* **158**, 198–212 (2014).
3. N. Schwartz *et al.*, *Science* **345**, 535–542 (2014).
4. M. Creed, V. J. Pascoli, C. Lüscher, *Science* **347**, 659–664 (2015).
5. S. M. Strittmatter, M. M. Lo, J. A. Javitch, S. H. Snyder, *Proc. Natl. Acad. Sci. U.S.A.* **81**, 1599–1603 (1984).
6. A. Saunders *et al.*, *Cell* **174**, 1015–1030.e16 (2018).
7. B. K. Atwood, D. A. Kupferschmidt, D. M. Lovinger, *Nat. Neurosci.* **17**, 540–548 (2014).
8. M. A. Ondetti, B. Rubin, D. W. Cushman, *Science* **196**, 441–444 (1977).
9. C. P. Blomeley, E. Bracci, *J. Neurosci.* **31**, 13346–13356 (2011).
10. B. P. Roques, M. C. Fournié-Zaluski, M. Wurm, *Nat. Rev. Drug Discov.* **11**, 292–310 (2012).
11. K. Ploj, E. Roman, L. Gustavsson, I. Nylander, *Brain Res. Bull.* **53**, 219–226 (2000).
12. A. Mansour, M. T. Hoversten, L. P. Taylor, S. J. Watson, H. Akil, *Brain Res.* **700**, 89–98 (1995).
13. C. E. Inturrisi *et al.*, *Proc. Natl. Acad. Sci. U.S.A.* **77**, 5512–5514 (1980).
14. M. Benuck, M. J. Berg, N. Marks, *Neurochem. Int.* **4**, 389–396 (1982).
15. R. Al-Hasani *et al.*, *eLife* **7**, e36520 (2018).
16. M. R. Banghart, S. Q. Neufeld, N. C. Wong, B. L. Sabatini, *Neuron* **88**, 1227–1239 (2015).
17. P. Charbogne *et al.*, *Biol. Psychiatry* **81**, 778–788 (2017).
18. M. K. Lobo *et al.*, *Science* **330**, 385–390 (2010).
19. J. W. Koo *et al.*, *Neuropsychopharmacology* **39**, 2646–2653 (2014).
20. V. Pascoli *et al.*, *Nature* **509**, 459–464 (2014).
21. E. S. Calipari *et al.*, *Proc. Natl. Acad. Sci. U.S.A.* **113**, 2726–2731 (2016).
22. V. Trezza, R. Damsteegt, E. J. Achterberg, L. J. Vanderschuren, *J. Neurosci.* **31**, 6362–6370 (2011).
23. H. Nam *et al.*, *Neuropsychopharmacology* **44**, 1876–1885 (2019).
24. H.-D. Kim *et al.*, *Mol. Psychiatry* **26**, 7316–7327 (2021).
25. O. Berton *et al.*, *Science* **311**, 864–868 (2006).
26. G. S. Zubenko, R. A. Nixon, *Am J. Psychiatry* **141**, 110–111 (1984).
27. R. F. Deicken, *Biol. Psychiatry* **21**, 1425–1428 (1986).
28. L. Germain, G. Chouinard, *Biol. Psychiatry* **23**, 637–641 (1988).
29. S. H. Croog *et al.*, *N. Engl. J. Med.* **314**, 1657–1664 (1986).
30. M. A. Testa, R. B. Anderson, J. F. Nackley, N. K. Hollenberg, Quality-of-Life Hypertension Study Group, *N. Engl. J. Med.* **328**, 907–913 (1993).
31. K. M. Sink *et al.*, *Arch. Intern. Med.* **169**, 1195–1202 (2009).

ACKNOWLEDGMENTS

We thank H. Lu and A. Daugherty (University of Kentucky) for generously providing the floxed ACE mouse line; A. Araque and A. D. Redish for helpful discussions; and the University of Minnesota Mouse Behavior Core for use of facilities to conduct behavioral tests. Some viral vectors used in this study were generated by the University of Minnesota Viral Vector and Cloning Core. Mass spectrometry was carried out in the Analytical Biochemistry Shared Resource of the Masonic Cancer Center, supported in part by NIH and the National Cancer Institute (Cancer Center Support Grant CA-77598). Schematics were created with BioRender.com. **Funding:** Supported by the University of Minnesota's MnDRIVE (Minnesota's Discovery, Research, and Innovation Economy) initiative (B.H.T., E.M.L., P.E.R.) and NIH grants T32DA007234 (B.H.T., C.T., D.D.B.), F30DA049476 (B.H.T.), F31MH122094 (C.T.), F30DA052109 (D.D.B.), F30MH124404 (A.K.), T32MH115886 (R.M.D.), and R01DA048946 and R21DA050120 (P.E.R.). **Author contributions:** Conceptualization: B.H.T. and P.E.R. Methodology and investigation: B.H.T., B.C.R., C.T., D.D.B., E.M.L., A.K., C.L.R., R.M.D., M.A.M., E.G., W.X., S.S.M., and P.E.R. Analysis and visualization: B.H.T., B.C.R., C.T., D.D.B., E.M.L., A.K., C.L.R., R.M.D., M.A.M., E.A.G., and Y.Z. Funding acquisition and project administration: P.E.R. Writing: B.H.T., B.C.R., C.T., D.D.B., E.M.L., A.K., C.L.R., R.M.D., M.A.M., E.A.G., W.X., Y.Z., S.S.M., and P.E.R. **Competing interests:** The authors declare that they have no competing interests. **Data and materials availability:** All data are available in the main text or the supplementary materials.

SUPPLEMENTARY MATERIALS

science.org/doi/10.1126/science.abl5130
Materials and Methods
Figs. S1 to S19
Tables S1 to S3
References (*32*–*65*)
MDAR Reproducibility Checklist
Data S1

View/request a protocol for this paper from *Bio-protocol*.

20 July 2021; accepted 9 February 2022
Published online 24 February 2022
10.1126/science.abl5130

Angiotensin-converting enzyme gates brain circuit–specific plasticity via an endogenous opioid

Brian H. Trieu, Bailey C. Remmers, Carlee Toddes, Dieter D. Brandner, Emilia M. Lefevre, Adrina Kocharian, Cassandra L. Retzlaff, Rachel M. Dick, Mohammed A. Mashal, Elysia A. Gauthier, Wei Xie, Ying Zhang, Swati S. More, and Patrick E. Rothwell

Science, **375** (6585), .
DOI: 10.1126/science.abl5130

Boosting endogenous opioid signaling

Angiotensin-converting enzyme (ACE) is expressed in brain tissue, but the central function of ACE in the brain has proven enigmatic. Trieu *et al*. discovered that ACE has a noncanonical role in governing endogenous opioid signaling in the brain. ACE cleaves and degrades an unconventional enkephalin called Met-enkephalin-Arg-Phe (MERF). Unlike conventional enkephalin pentapeptides, MERF is selectively degraded by ACE and enhances μ-opioid receptor activation in the nucleus accumbens, perhaps explaining its antidepressant effects in patients taking ACE inhibitors. — PRS